From $Ba[Sn(IO_3)_6]$ to $Ba[Sn(IO_3)_4F_2]$: Fluoride-Ion-Driven Enhancement of Birefringence and Band Gap

Xue-Ying Zhang,[a,b] Peng-Fei Chen,[c] Bing-Ping Yang[a,b] and Jiang-Gao Mao[a,b]*

[a]State Key Laboratory of Functional Crystals and Devices, Fujian Institute of Research on the Structure of Matter, Chinese Academy of Sciences, Fuzhou 350002, China.

[b]University of Chinese Academy of Sciences, Beijing, 100049, China.

[c]Research Institute of Optoelectronic Functional Materials, Department of Physics and Information Engineering, Jining University, Qufu, Shandong 273155, P. R. China.

Table of contents

S1 Experimental Methods

Reagents and synthesis

Barium iodate monohydrate ($Ba(IO_3)_2·H_2O$, 99%), stannous chloride ($SnCl_2$, 99%), periodic acid (H_5IO_6, 99%), and hydrofluoric acid (HF, 40% aqueous solution) were employed as the starting reactants. Hydrofluoric acid is a highly corrosive substance and operators must use personal protective equipment and follow standard operating procedures when handling it. All chemicals were purchased from Aladdin Biochemical Technology Co., Ltd and used without further purification.

For the synthesis of $Ba[Sn(IO_3)_6]$, a mixture of $Ba(IO_3)_2·H_2O$ (0.3 mmol, 0.152 g), $SnCl_2$ (0.3 mmol, 0.057 g), H_5IO_6 (3.0 mmol, 0.684 g), 0.5 mL HF, and 2 mL deionized water was prepared. In the case of $Ba[Sn(IO_3)_4F_2]$, the reaction mixture consisted of $Ba(IO_3)_2·H_2O$ (1.0 mmol, 0.505 g), $SnCl_2$ (1.0 mmol, 0.190 g), H_5IO_6 (2.0 mmol, 0.456 g), 0.5 mL HF, and 2 mL deionized water. Each mixture was transferred into a 23 mL Teflon-lined autoclave, which was then hermetically sealed and heated at 230 ℃ for 72 h, followed by programmed cooling to ambient temperature at a rate of 5 ℃ h^{-1}. Colorless transparent block crystals of $Ba[Sn(IO_3)_6]$ and white transparent crystals of $Ba[Sn(IO_3)_4F_2]$ were obtained with Sn-based yields of approximately 90% and 65%, respectively. The phase purity of both products was confirmed via powder X-ray diffraction (XRD) measurements (Figure S1).

Single-crystal structure determination

Single-crystal X-ray diffraction data of the target compounds were collected on an Agilent Technologies SuperNova dual-wavelength CCD diffractometer with Mo Kα radiation (λ=0.71073 Å) at 293 K. Data reduction was conducted using the CrysAlisPro software package. Numerical absorption correction based on Gaussian integration over a multifaceted crystal model and empirical absorption correction using spherical harmonics implemented in the SCALE3 ABSPACK scaling algorithm were carried out.[1] The structures of $Ba[Sn(IO_3)_6]$ and $Ba[Sn(IO_3)_4F_2]$ were solved by direct methods and refined via full-matrix least-squares calculations on F^2 using the SHELXL-2017 program.[2] All non-hydrogen atoms were refined with anisotropic thermal parameters. Symmetry checks for both structures were performed using PLATON software, and no missing symmetry elements were identified.[3] Crystallographic data and structural refinement parameters are summarized in Table S1, while fractional atomic coordinates and selected bond lengths are presented in Tables S2−S5.

Powder X-ray diffraction (PXRD)

The powder X-ray diffraction data of the samples were collected using a Rigaku MiniFlex 600 X-ray powder diffractometer equipped with Cu Kα radiation (λ = 1.54186 Å) at room temperature. The scan range is 10–70°, the scan step is 0.02°, and the scan speed is 3° min^{-1}. Simulated powder X-ray diffraction patterns were generated using Mercury 3.7.

Energy-dispersive X-ray spectroscopy (EDS)

Microprobe elemental analysis was carried out using a field emission scanning electron microscope (JSM6700F) equipped with an energy-dispersive X-ray spectrometer (Oxford INCA).

Spectroscopic measurements

The infrared (IR) spectrum of the sample was measured using a Nicolet Magna 750 FT-IR spectrometer in the range of 4000–400 cm^{-1}. The sample was prepared as a pellet with KBr powder. The ultraviolet-visible-near-IR (UV-vis-NIR) diffuse reflectance spectrum was recorded using a PerkinElmer Lambda 950 UV-vis-NIR spectrophotometer in the range of 2500–200 nm

with $BaSO_4$ powder as the reference substrate for 100% reflectance. The diffuse reflectance data were converted into absorbance data using the Kubelka–Munk function $\alpha/S = (1 - R)^2/2R$, where α is the absorption coefficient, S is the scattering coefficient, and R is the reflectance.[4] In the α/S versus energy plot, the band gap value was obtained by extrapolating the absorption edge to the baseline.

Thermal analysis

Thermogravimetric analysis (TGA) and differential thermal analysis (DTA) of the samples were performed using a NETZCH STA 449F3 thermal analyses. The sample was placed in a custom-made Al_2O_3 crucible and heated from 20 ℃ to 1000 ℃ under a N_2 atmosphere at a heating rate of 10 ℃ min^{-1}, using an empty crucible as a reference.

Computational Methods

The electronic and optical properties of $Ba[Sn(IO_3)_6]$ and $Ba[Sn(IO_3)_4F_2]$ were calculated with CASTEP using density functional theory (DFT) and the plane wave pseudopotential method.[5, 6] The generalised gradient approximation Perdew–Burke–Ernzerhof (PBE) exchange–correlation functional was used.[7] The core–electron interactions were described by the norm-conserving pseudopotential. The valence electron configurations considered were: Ba $5s^25p^66s^2$, Sn $5s^25p^2$, I $5s^25p^5$, O $2s^22p^4$, and F $2s^22p^5$. Cutoff energies of 750 eV and 850 eV were selected for $Ba[Sn(IO_3)_6]$ and $Ba[Sn(IO_3)_4F_2]$, respectively, to optimize the plane-wave basis set. Monkhorst−Pack k-point meshes of 1×1×2 and 3×3×1 were employed for Brillouin zone integration of $Ba[Sn(IO_3)_6]$ and $Ba[Sn(IO_3)_4F_2]$, respectively. The optical properties were calculated with >200 empty bands to ensure accuracy. All other computational parameters and convergence criteria followed the default settings of the CASTEP package. Gaussian 09 was mainly employed to calculate the polarizability anisotropy (δ) of the microscopic units. Density functional theory was selected as the calculation method, and 6-31G/LANL2DZ was used as the basis set. Multiwfn was used to extract the polarizability anisotropy in the Gaussian 09 output file.

Table S1. Crystallographic data and structure refinement parameters of $Ba[Sn(IO_3)_6]$ and $Ba[Sn(IO_3)_4F_2]$.

Formula	$Ba[Sn(IO_3)_6]$	$Ba[Sn(IO_3)_4F_2]$
Formula weight	1305.43	993.63
Temperature/K	295.3(4)	296.15
Crystal system	trigonal	monoclinic
Space group	*R*-3	*C*2/*c*
a/Å	11.0257(13)	14.4425(13)
b/Å	11.0257(13)	5.2898(5)
c/Å	11.101(2)	18.1768(12)
α/°	90	90
β/°	90	112.868(6)
γ/°	120	90
V/Å^3	1168.7(4)	1279.52(19)
Z	3	4
ρ_{calc}g/cm^3	5.564	5.158
μ/mm^{-1}	16.101	14.747
F(000)	1704.0	1728.0
Radiation	Mo Kα (λ = 0.71073)	Mo Kα (λ = 0.71073)
Goodness-of-fit on F^2	1.068	1.050
R_1, wR_2 [I>=2σ (I)]	0.0245, 0.0521	0.0237, 0.0529
R_1, wR_2 (all data)	0.0285, 0.0551	0.0263, 0.0543

[a] $R_1 = \Sigma||F_o|-|F_c||/\Sigma|F_o|$; and $wR_2 = \{\Sigma[w(F_o^2-F_c^2)^2]/\Sigma[w(F_o^2)^2]\}^{1/2}$

Table S2. Fractional atomic coordinates ($\times 10^4$), equivalent isotropic displacement parameters ($Å^2 \times 10^3$) and bond valence sums (BVS) of $Ba[Sn(IO_3)_6]$. U_{eq} is defined as 1/3 of the trace of the orthogonalised U_{ij} tensor.

Atom	*x*	*y*	*z*	U(eq)	BVS
Ba1	6666.67	3333.33	3333.33	11.0(3)	2.444
I1	3740.2(5)	4441.6(5)	3796.3(4)	10.5(3)	4.999
Sn1	3333.33	6666.67	1666.67	10.8(3)	3.979
O1	5077(5)	4613(5)	2784(4)	16.4(12)	2.033
O2	4681(5)	6039(5)	4657(5)	15.6(12)	1.865
O3	2779(5)	4924(5)	2709(4)	12.1(11)	2.171

The BVS were calculated using the equation: $V_i=\sum_j S_{ij}=\sum_j exp[(r_0—r_{ij})/B]$, where V_i is the oxidation state of cation i, S_{ij} is the valence of the bond between the cation i and the anion j, r_0 and r_{ij} are the empirically determined bond length parameter and experimentally measured bond length, respectively. The empirically determined parameter B was set to 0.37.[8]

Table S3. Selected bond lengths of $Ba[Sn(IO_3)_6]$.

Bond	Length/Å	Bond	Length/Å
Ba1−O1[1]	2.811(5)	Ba1−O2[11]	2.948(5)
Ba1−O1[2]	2.811(5)	I1−O3	1.851(5)
Ba1−O1[3]	2.811(5)	I1−O1	1.787(5)
Ba1−O1[4]	2.811(5)	I1−O2	1.807(5)
Ba1−O1[5]	2.811(5)	Sn1−O3	2.057(5)
Ba1−O1	2.811(5)	Sn1−O3[12]	2.057(5)
Ba1−O2[6]	2.948(5)	Sn1−O3[13]	2.057(5)
Ba1−O2[7]	2.948(5)	Sn1−O3[14]	2.057(5)
Ba1−O2[8]	2.948(5)	Sn1−O3[15]	2.057(5)
Ba1−O2[9]	2.948(5)	Sn1−O3[16]	2.057(5)
Ba1−O2[10]	2.948(5)		

Symmetry transformations for the atoms generated: [1]4/3-X, 2/3-Y, 2/3-Z; [2]1+Y-X, 1-X, +Z; [3]1-Y, +X-Y, +Z; [4]1/3+Y, 2/3-X+Y, 2/3-Z; [5]1/3-Y+X, -1/3+X, 2/3-Z; [6]+Y, -X+Y, 1-Z; [7]4/3-Y, 2/3+X-Y, -1/3+Z; [8]1-Y+X, +X, 1-Z; [9]1-X, 1-Y, 1-Z; [10]1/3+Y-X, 2/3-X, -1/3+Z; [11]1/3+X, -1/3+Y, -1/3+Z; [12]-1/3+Y, 1/3-X+Y, 1/3-Z; [13]2/3-X, 4/3-Y, 1/3-Z; [14]+Y-X, 1-X,+Z; [15]2/3-Y+X, 1/3+X, 1/3-Z; [16]1-Y, 1+X-Y, +Z.

Table S4. Fractional atomic coordinates ($\times 10^4$), equivalent isotropic displacement parameters ($Å^2 \times 10^3$) and bond valence sums (BVS) of $Ba[Sn(IO_3)_4F_2]$. U_{eq} is defined as 1/3 of the trace of the orthogonalised U_{ij} tensor.

Atom	*x*	*y*	*z*	U(eq)	BVS
Ba1	0	19330.8(10)	7500	11.58(17)	1.979
I1	3007.8(3)	8202.6(7)	8380.4(2)	10.08(16)	5.113
I2	6352.6(3)	9137.1(7)	9266.9(2)	10.74(16)	5.083
Sn1	5000	5000	10000	8.46(18)	4.265
F1	4889(3)	6425(6)	10961.2(18)	15.9(8)	0.717
O1	6996(4)	6323(8)	9191(3)	20.3(10)	1.788
O2	5257(3)	8920(8)	8361(2)	18.7(10)	2.005
O3	5773(3)	8132(7)	9965(2)	13.9(10)	2.263
O4	3317(3)	6145(8)	7727(2)	18.5(10)	2.030
O5	1798(3)	6888(8)	8207(2)	15.0(9)	2.071
O6	3635(3)	6633(8)	9350(2)	15.5(10)	2.235

Table S5. Selected bond lengths of $Ba[Sn(IO_3)_4F_2]$.

Bond	Length/Å	Bond	Length/Å
Ba1−F1[1]	2.768(3)	I1−O6	1.838(4)
Ba1−F1[2]	2.768(3)	I2−O1	1.788(4)
Ba1−O2[1]	2.834(4)	I2−O2	1.790(4)
Ba1−O2[2]	2.834(4)	I2−O3	1.849(4)
Ba1−O4[1]	2.789(4)	Sn1−F1[9]	1.966(3)
Ba1−O4[2]	2.789(4)	Sn1−F1	1.966(3)
Ba1−O5[7]	2.733(4)	Sn1−O3[9]	2.013(4)
Ba1−O5[8]	2.733(4)	Sn1−O3	2.013(4)
I1−O4	1.791(4)	Sn1−O6[9]	2.054(4)
I1−O5	1.791(4)	Sn1−O6	2.054(4)

Symmetry transformations for the atoms generated: [1]-1/2+X, 3/2+Y,+Z; [2]1/2-X, 3/2+Y, 3/2-Z; [3]1/2-X, 5/2-Y, 2-Z; [4]-1/2+X, 5/2-Y, -1/2+Z; [5]-1/2+X, 1/2+Y, +Z; [6]1/2-X, 1/2+Y, 3/2-Z; [7]+X, 1+Y, +Z; [8]-X, 1+Y, 3/2-Z; [9]1-X, 1-Y, 2-Z.

Table S6. Comparison of band gaps and birefringence among partial compounds.

Compound	Band gap (eV)	Birefringence	Ref.
$RbIO_3$	4.00	N/A	9
$RbIO_2F_2$	4.20	N/A	9
$CsIO_3$	4.20	0.19 at 1064 nm	10
$CsIO_2F_2$	4.50	0.046 at 1064 nm	10
$BiO(IO_3)$	3.30	N/A	11
$Bi_2(IO_4)(IO_3)_3$	3.30	0.196 at 1064 nm	12
$Bi_3OF_3(IO_3)_4$	3.70	0.057 at 532 nm	13
$Bi(IO_3)F_2$	3.97	0.209 at 1064 nm	14
$Sn(IO_3)_4$	3.96	N/A	15
$Sn(IO_3)_2F_2$	4.08	0.234 at 1064 nm	15
$Ba[Sn(IO_3)_6]$	**3.97**	**0.120@532nm**	This work
$Ba[Sn(IO_3)_4F_2]$	**4.17**	**0.214@532nm**	This work
$K_2BiI_5O_{15}$	3.50	0.0536 at 1064 nm	16
$KBi_2(IO_3)_2F_5$	3.75	N/A	17
$Rb_2BiI_5O_{15}$	3.53	0.0427 at 1064 nm	16
$RbBi_2(IO_3)_2F_5$	3.78	N/A	17
$(NH_4)Bi_2(IO_3)_2F_5$	3.88	0.069@589.3nm	18
$HBa_{2.5}(IO_3)_6(I_2O_5)$	3.63	N/A	19
$HBa(I_4O_{11})(IO_3)$	3.78	N/A	19
$Ba(IO_3)F$	4.32	0.1253 at 589.3 nm	20
$NaGa(IO_3)_4$	4.83	0.23 at 1064 nm	21
$NaGa(IO_3)_2F_2$	4.86	0.21 at 1064 nm	21
$Ce(IO_3)_4$	2.17	0.039 at 546 nm	22
$Ce(IO_3)_2F_2$	2.70	0.140@1064nm	22
$Ce(IO_3)_3F$	2.55	0.130@1064nm	23
$Li_2Ce(IO_3)_4F_2$	2.76	0.054@589nm	24
$Ce(IO_3)_2F_2·H_2O$	2.60	0.046@1064nm	25
$ZrF_2(IO_3)_2$	4.24	0.329@1064nm	26
$LaZr(IO_3)_5F_2$	4.13	0.082@1064nm	27
$CsZrF_4(IO_3)$	4.35	0.200@1064nm	28
$CsHfF_4(IO_3)$	4.47	0.161@532nm	29
$RbGaF_3(IO_3)$	4.61	0.174@1064nm	26
$LiGaF_2(IO_3)_2$	4.33	0.206@532nm	30
$Ba[InF_3(IO_3)_2]$	4.35	0.205@532nm	31
$Ba[FeF_4(IO_3)]$	3.82	0.062@532nm	32
$Ba_2[FeF_4(IO_3)_2]IO_3$	3.90	0.141@532nm	32
$Cd_3(IO_3)(IO_4)F_2·0.1CdO$	4.03	0.133@546.1nm	33
$CdIO_3F$	4.22	0.072@1064 nm	34
$ZnIO_3F$	4.20	0.230@532nm	34

[a]N/A = not applicable or not available.

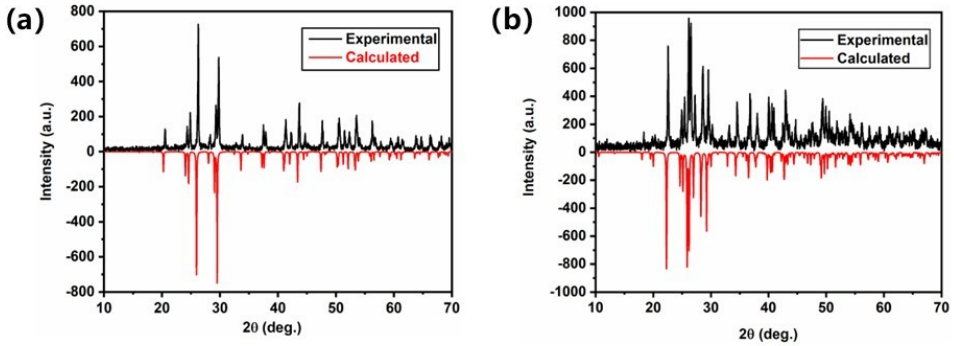

Figure S1. Experimental and simulated powder X-ray diffraction (PXRD) patterns of $Ba[Sn(IO_3)_6]$ (a) and $Ba[Sn(IO_3)_4F_2]$ (b).

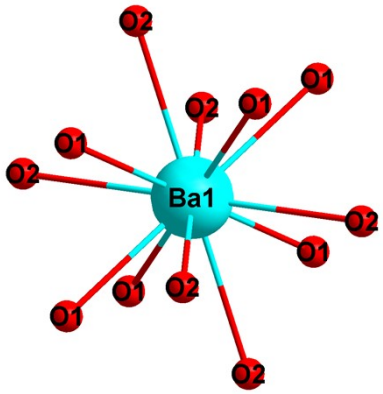

Figure S2. Coordination environment of Ba^{2+} in $Ba[Sn(IO_3)_6]$.

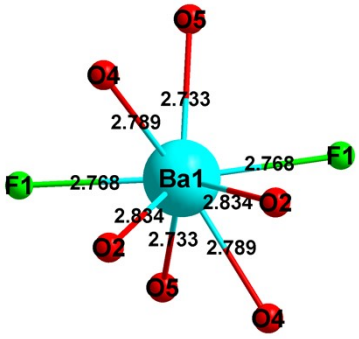

Figure S3. Coordination environment of Ba^{2+} in $Ba[Sn(IO_3)_4F_2]$.

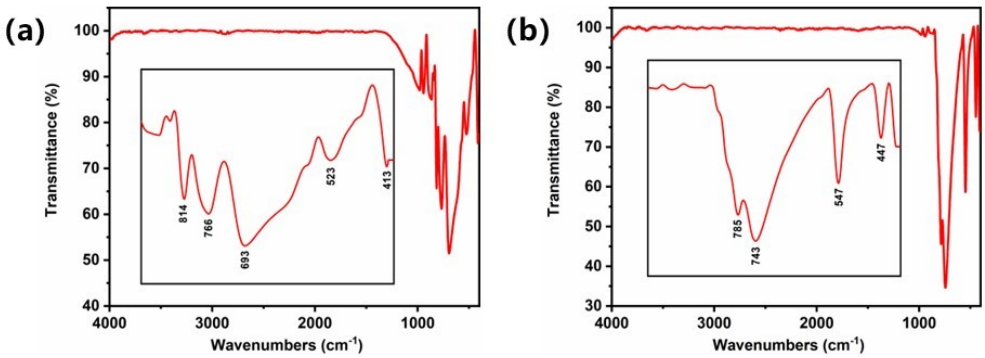

Figure S4. IR spectra of $Ba[Sn(IO_3)_6]$ (a) and $Ba[Sn(IO_3)_4F_2]$ (b).

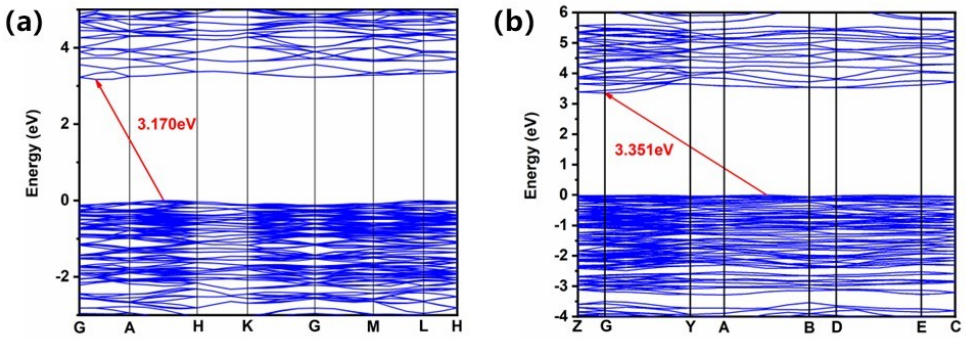

Figure S5. Calculated band structures of $Ba[Sn(IO_3)_6]$ (a) and $Ba[Sn(IO_3)_4F_2]$ (b).

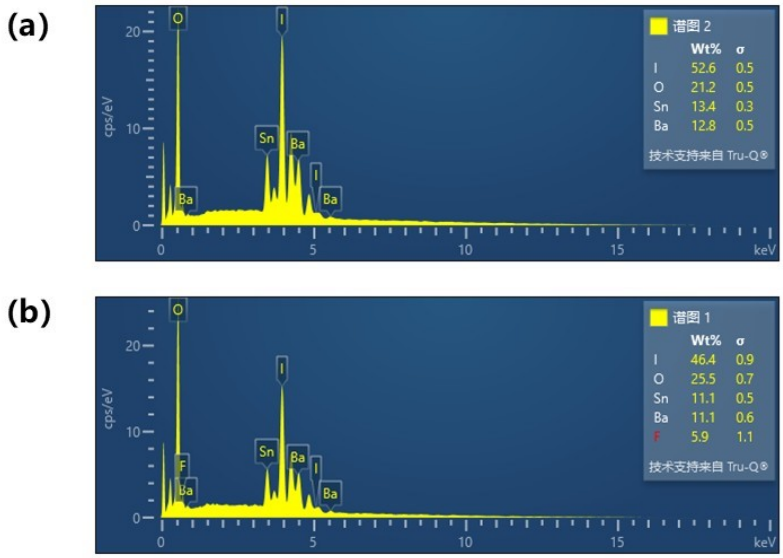

Figure S6. Energy dispersive spectroscopy analysis of $Ba[Sn(IO_3)_6]$ (a) and $Ba[Sn(IO_3)_4F_2]$ (b).

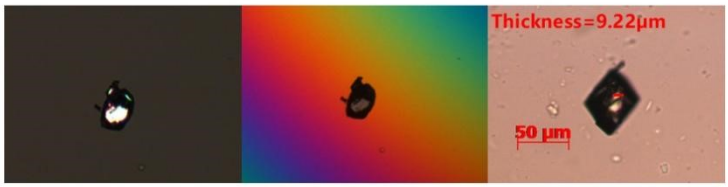

Figure S7. Experimental birefringence at 546 nm for $Ba[Sn(IO_3)_6]$.

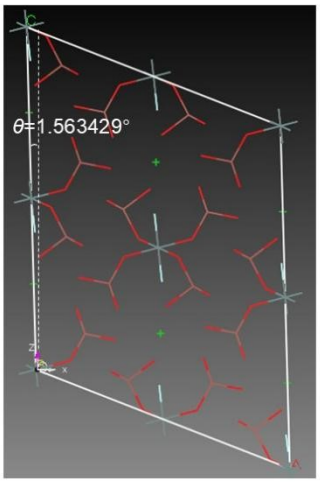

Figure S8. Distribution of the rotated *ac* plane and diagonalized dielectric tensor axes of $Ba[Sn(IO_3)_4F_2]$.

References

(1) Blessing, R. H. An Empirical Correction for Absorption Anisotropy. *Acta Crystallogr A* **1995**, *51*, 33-38.

(2) Sheldrick, G. M. SHELXT - integrated space-group and crystal-structure determination. *Acta Crystallogr A Found Adv* **2015**, *71* (Pt 1), 3-8.

(3) Spek, A. L. Single-crystal structure validation with the program PLATON. *J. Appl. Crystallogr.* **2003**, *36*, 7-13.

(4) Kubelka; Munk. The Kubelka-Munk Theory of Reflectance. *Zeit. Für Tekn. Physik* **1931**, *12*, 593.

(5) Milman, V.; Winkler, B.; White, J. A.; Pickard, C. J.; Payne, M. C.; Akhmatskaya, E. V.; Nobes, R. H. Electronic structure, properties, and phase stability of inorganic crystals: A pseudopotential plane-wave study. *Int. J. Quantum Chem.* **2000**, *77* (5), 895-910.

(6) Segall, M. D.; Lindan, P. J. D.; Probert, M. J.; Pickard, C. J.; Hasnip, P. J.; Clark, S. J.; Payne, M. C. First-principles simulation: ideas, illustrations and the CASTEP code. *J Phys-Condens Mat* **2002**, *14* (11), 2717-2744.

(7) Perdew, J. P.; Burke, K.; Ernzerhof, M. Generalized gradient approximation made simple. *Phys. Rev. Lett.* **1996**, *77* (18), 3865-3868.

(8) Brown, I. D.; Altermatt, D. Bond-Valence Parameters Obtained from a Systematic Analysis of the Inorganic Crystal-Structure Database. *Acta Crystallogr., Sect. B: Struct. Sci.* **1985**, *41*, 244-247.

(9) Wu, Q.; Liu, H. M.; Jiang, F. C.; Kang, L.; Yang, L.; Lin, Z. S.; Hu, Z. G.; Chen, X. G.; Meng, X. G.; Qin, J. G. $RbIO_3$ and $RbIO_2F_2$: Two Promising Nonlinear Optical Materials in Mid-IR Region and Influence of Partially Replacing Oxygen with Fluorine for Improving Laser Damage Threshold. *Chem. Mater.* **2016**, *28* (5), 1413-1418.

(10) Zhang, M.; Hu, C.; Abudouwufu, T.; Yang, Z. H.; Pan, S. L. Functional Materials Design via Structural Regulation Originated from Ions Introduction: A Study Case in Cesium Iodate System. *Chem. Mater.* **2018**, *30* (3), 1136-1145.

(11) Zhang, J.; Du, X. H.; Ke, S. H.; Xu, B.; Zheng, G. H.; Rowlands, D. A.; Yao, K. L. Dielectric, piezoelectric and nonlinear optical properties of polar iodate $BiO(IO_3)$ from first-principles studies. *J. Solid State Chem.* **2020**, *281*, 121057-121067.

(12) Cao, Z. B.; Yue, Y. C.; Yao, J. Y.; Lin, Z. S.; He, R.; Hu, Z. G. $Bi_2(IO_4)(IO_3)_3$: A New Potential Infrared Nonlinear Optical Material Containing $[IO_4]^{3-}$ Anion. *Inorg. Chem.* **2011**, *50* (24), 12818-12822.

(13) Zhang, M.; Su, X.; Mutailipu, M.; Yang, Z. H.; Pan, S. L. $Bi_3OF_3(IO_3)_4$: Metal Oxyiodate Fluoride Featuring a Carbon-Nanotube-like Topological Structure with Large Second Harmonic Generation Response. *Chem. Mater.* **2017**, *29* (3), 945-949.

(14) Mao, F. F.; Hu, C. L.; Xu, X.; Yan, D.; Yang, B. P.; Mao, J. G. $Bi(IO_3)F_2$: The First Metal Iodate Fluoride with a Very Strong Second Harmonic Generation Effect. *Angew. Chem. Int. Ed.* **2017**, *56* (8), 2151-2155.

(15) Luo, M.; Liang, F.; Hao, X.; Lin, D. H.; Li, B. X.; Lin, Z. S.; Ye, N. Rational Design of the Nonlinear Optical Response in a Tin Iodate Fluoride $Sn(IO_3)_2F_2$. *Chem. Mater.* **2020**, *32* (6), 2615-2620.

(16) Huang, Y.; Meng, X. G.; Gong, P. F.; Yang, L.; Lin, Z. S.; Chen, X. G.; Qin, J. G. $A_2BiI_5O_{15}$ ($A = K^+$ or Rb^+): two new promising nonlinear optical materials containing $[I_3O_9]^{3-}$ bridging anionic groups. *J. Mater. Chem. C* **2014**, *2* (20), 4057-4062.

(17) Liu, H. M.; Wu, Q.; Jiang, X. X.; Lin, Z. S.; Meng, X. G.; Chen, X. G.; Qin, J. G. $ABi_2(IO_3)_2F_5$

(A=K, Rb, and Cs): A Combination of Halide and Oxide Anionic Units To Create a Large Second‐Harmonic Generation Response with a Wide Bandgap. *Angew. Chem. Int. Ed.* **2017**, *56* (32), 9492-9496.

(18) Fan, H. X.; Lin, C. S.; Chen, K. C.; Peng, G.; Li, B. X.; Zhang, G.; Long, X. F.; Ye, N. $(NH_4)Bi_2(IO_3)_2F_5$: An Unusual Ammonium‐Containing Metal Iodate Fluoride Showing Strong Second Harmonic Generation Response and Thermochromic Behavior. *Angew. Chem. Int. Ed.* **2020**, *59* (13), 5268-5272.

(19) Mao, F. F.; Hu, C. L.; Chen, J.; Wu, B. L.; Mao, J. G. $HBa_{2.5}(IO_3)_6(I_2O_5)$ and $HBa(IO_3)(I_4O_{11})$: Explorations of Second-Order Nonlinear Optical Materials in the Alkali-Earth Polyiodate System. *Inorg. Chem.* **2019**, *58* (6), 3982-3989.

(20) Fan, H.; Peng, G.; Lin, C. S.; Chen, K. C.; Yang, S. D.; Ye, N. $Ba(IO_3)F$: An Alkaline-Earth-Metal Iodate Fluoride Crystal with Large Band Gap and Birefringence. *Inorg. Chem.* **2020**, *59* (11), 7376-7379.

(21) Yang, S. X.; Wu, H. P.; Hu, Z. G.; Wang, J. Y.; Wu, Y. C.; Yu, H. W. From $NaGa(IO_3)_3F$ to $NaGa(IO_3)_2F_2$ and $NaGa(IO_3)_4$: The Effects of Chemical Substitution between F^- Anions and IO_3^- Groups on the Structures and Properties of Gallium Iodates. *Inorg. Chem.* **2024**, *63* (2), 1404-1413.

(22) Wu, T. H.; Jiang, X. X.; Wu, C.; Sha, H. Y.; Wang, Z. J.; Lin, Z. S.; Huang, Z. P.; Long, X. F.; Humphrey, M. G.; Zhang, C. From $Ce(IO_3)_4$ to $CeF_2(IO_3)_2$: fluorinated homovalent substitution simultaneously enhances SHG response and bandgap for mid-infrared nonlinear optics. *J. Mater. Chem. C* **2021**, *9* (28), 8987-8993.

(23) Ma, N.; Huang, Y.; Hu, C. L.; Zhang, M. Z.; Li, B. X.; Mao, J. G. $Ce(IO_3)_3F$ and $Ce(IO_3)_2(NO_3)$: Two Mixed-Anion Cerium Iodates with Good Nonlinear Optical and Birefringent Properties. *Inorg. Chem.* **2023**, *62* (37), 15329-15333.

(24) Tang, C. C.; Jiang, X. X.; Guo, S.; Guo, R. X.; Liu, L. J.; Xia, M. J.; Huang, Q.; Lin, Z. S.; Wang, X. Y. Synthesis, Crystal Structure, and Optical Properties of the First Alkali Metal Rare-Earth Iodate Fluoride: $Li_2Ce(IO_3)_4F_2$. *Cryst. Growth Des.* **2020**, *20* (4), 2135-2140.

(25) Abudouwufu, T.; Zhang, M.; Cheng, S. C.; Yang, Z. H.; Pan, S. L. $Ce(IO_3)_2F_2{\cdot}H_2O$: The First Rare‐Earth‐Metal Iodate Fluoride with Large Second Harmonic Generation Response. *Chem. Eur.J.* **2019**, *25* (5), 1221-1226.

(26) Chen, J.; Du, K. Z. $ZrF_2(IO_3)_2$ and $RbGaF_3(IO_3)$: Two Promising Birefringent Crystals Featuring 1D Metal-Fluoride Cationic Chains and Wide Bandgaps. *Inorg. Chem.* **2022**, *61* (44), 17893-17901.

(27) Mao, F. F.; Liu, J. D.; Hu, J. Y.; Wu, H. From $Ag_2Zr(IO_3)_6$ to $LaZr(IO_3)_5F_2$: A Case of Constructing Wide‐band‐gap Birefringent Materials through Chemical Cosubstitution. *Chem. Asian J.* **2020**, *15* (21), 3487-3493.

(28) Lin, L.; Jiang, X. X.; Wu, C.; Lin, Z. S.; Huang, Z. P.; Humphrey, M. G.; Zhang, C. $CsZrF_4(IO_3)$: The First Polar Zirconium Iodate with cis-$[ZrO_2F_6]$ Polyhedra Inducing Optimized Balance of Large Band Gap and Second Harmonic Generation. *Chem. Mater.* **2021**, *33* (14), 5555-5562.

(29) Huang, Y.; Li, B. X.; Hu, C. L.; Yang, B. P.; Mao, J. G. $CsHfF_4(IO_3)$: A Hafnium Iodate Exhibiting a Strong Second-Harmonic-Generation Effect and a Wide Band Gap Achieved by Mixed-Ligand Acentric Coordination. *Inorg. Chem.* **2023**, *62* (8), 3343-3348.

(30) Chen, J.; Hu, C. L.; Mao, J. G. $LiGaF_2(IO_3)_2$: A mixed-metal gallium iodate-fluoride with large birefringence and wide band gap. *Sci. China Mater.* **2020**, *64* (2), 400-407.

(31) Jiang, X. Q.; Wu, H. P.; Yu, H. W.; Hu, Z. G.; Wang, J. Y.; Wu, Y. C. Synthesis, Structure,

Characterization, and Calculation of a Noncentrosymmetric Fluorine-Containing Indium Iodate, $Ba[InF_3(IO_3)_2]$. *Cryst. Growth Des.* **2021**, *21* (7), 4005-4012.

(32) Huang, Q. M.; Hu, C. L.; Yang, B. P.; Fang, Z.; Huang, Y.; Mao, J. G. $Ba_2[FeF_4(IO_3)_2]IO_3$: a promising nonlinear optical material achieved by chemical-tailoring-induced structure evolution. *Chem. Commun.* **2021**, *57* (87), 11525-11528.

(33) Cao, L. L.; Zhang, S. Z.; Zhao, D.; Li, B. X.; Yan, T.; Yang, G. S.; Lin, Z. S.; Luo, M.; Ye, N. $Cd_3(IO_3)(IO_4)F_2 \cdot 0.1CdO$: A Nonlinear-Optical Crystal with the Introduction of Fluoride into Iodate Containing Both $[IO_3]^-$ and $[IO_4]^{3-}$ Groups. *Inorg. Chem.* **2021**, *60* (8), 6040-6046.

(34) Cao, L. L.; Luo, M.; Lin, C. S.; Zhou, Y. Q.; Zhao, D.; Yan, T.; Ye, N. From centrosymmetric to noncentrosymmetric: intriguing structure evolution in d^{10}-transition metal iodate fluorides. *Chem. Commun.* **2020**, *56* (73), 10734-10737.